Optimization of the active absorber scheme for the protection of the Dispersion Suppressor

Magistris M., Santana Leitner M., Assmann R., Bracco C., Brugger M., Cerutti F., Ferrari A., Redaelli S., Vlachoudis V.

December 2006

Abstract

There are two main types of cold elements in IR7: quadrupole and dipole magnets (MQ and MB). According to predictions, these objects are to lose their superconducting properties if the spurious power densities reach about 1 and 5 $\frac{mW}{cm^3}$, respectively. In order to protect these fragile components, 5 active absorbers (TCLA) were designed and a systematic study was launched to maximize the shielding efficiency of the absorber system for different configurations (locations and orientations). The TCLA's are identical to the secondary collimators (TCS), the only difference is found in the material of the jaw, which, initially, was set integrally to Cu (instead of C) and later included a small W insertion. This report summarizes the survey of cold element protection through TCLA insertion optimization.

Keywords: betatron cleaning insertion, tertiary halo, power deposition, cold magnets' quench, active absorbers (TCLA)

This is an internal CERN publication and does not necessarily reflect the views of the LHC project management

LHC-Project-Note-423
28/07/2009

Contents

1 Introduction

1.1 Simulations of the IR7 insertion

The collimation system of the future Large Hadron Collider (LHC) at CERN is a challenging project since the transverse intensities of the LHC beams are three orders of magnitude greater than those of other current facilities. Two insertions (IR3, IR7) of the LHC are dedicated to beam cleaning with the design goal of absorbing most of the primary beam halo and its secondary radiation. The full collimation system (including the beam cleaning insertions as well as other locations around the machine) will house more than 100 movable collimators, and will partly be among the most radioactive areas of the LHC. The collimators have to withstand the deposited power, which for collimation layout phase I can reach values of about 25 kW in the most affected collimator ($\sim$3 kW in the jaws only).

The created tertiary halo escaping the collimation system in IR7 risks to damage downstream beam elements, e.g., heat up cold magnets up to unacceptable levels and causing a quench, if no additional absorber were used. In order to assess the energy deposition in sensitive components, extensive simulations were run with the Monte Carlo cascade code FLUKA [1, 2].

The here presented results, as well as all FLUKA IR7 calculations which are based on pre-calculated loss patterns, rely on tracking simulations, whose output is used as direct input for FLUKA where the respective loss locations are then sampled and used as starting point of inelastic (non-elastic and single-diffractive) interactions.

1.2 Input from proton beam simulations

Proton losses in the LHC aperture are simulated by special accelerator physics simulations. These simulations typically track 5 10^6 protons over at least 200 turns. Initial impacts from primary beam halo are taking place at the primary collimators. Secondary, tertiary and quartiary beam halo develops through multiple interactions in the 44 collimators per ring. With a resolution of 10 cm it is checked that the tracked protons are not touching the available LHC aperture. The tracking of a single proton is stopped once it hits an aperture limit and experiences an inelastic interaction. The proton coordinates of inelastic interactions are saved and later used as input to the FLUKA studies on energy deposition. This input depends on detailed beam conditions, number and settings of collimators, imperfections, halo models and the accelerator optics. The provided input is characterized below:

1. Beam parameters: Beam energy of 450 GeV and 7 TeV, nominal beam emittances, nominal energy spread.

Energy	β^* IR1-IR5 [m]	β^* IR2-IR8 [m]
450 GeV	17	11
7 TeV	0.55	11

Table 1: β-values for injection and fully squeezed optics in the four interaction points.

	Half gap [σ_r]	
Collimator family	Injection	Low Beta
TCP-IR7	5.7	6
TCSG-IR7	6.7	7
TCLA-IR7	10	10
TCP-IR3	8	15
TCSG-IR3	9.3	18
TCLA-IR3	10	20
TCTH/V-IR1/2/5/8	99	8.3
TCL-IR1/5	99	10
TDI-TCLI-IR2/8	6.8	99
TCSG-IR6	7	7.5
TCDQ-IR6	8	8

Table 2: Collimator apertures for injection and fully squeezed optics.

2. Accelerator optics: LHC optics V6.500 (see Table 1), zero orbit, design tunes, corrected chromaticity. No misalignments and no field errors.

3. Number and settings of collimators (see [3] and references therein): Full phase 1 system. IR7 nominal settings as in Table 2. Azimuthal orientation following collimation system design. Collimators at other insertions (IR1, 2, 3, 5, 6, 8) were used in tracking at nominal settings for the injection and fully squeezed optics (see Table 2). No imperfections were included for setup errors, jaw surface non-flatness and aperture model.

4. Halo model: As IR7 is the betatron cleaning insertion we only studied betatron halo losses. The work on optimization of the active absorber scheme was performed with input for horizontal, vertical and skew primary beam halo.

The input from proton simulations was defined in order to determine the ideal performance reach of the betatron cleaning system in IR7, including optimized active absorbers. The loss maps refer to the case of a fully installed IR7 system at its final settings and after correction of imperfections. The data should not be used

for predictions of losses in the first years of the LHC. Early on in LHC operation less collimators will be used at larger openings (larger β^* and lower intensity) and imperfections will have a large impact (lower efficiency initially).

1.3 Scheme of work

The scheme of the simulations has followed the priorities and setup changes at each point of the project. It was decided firstly to determine the *active* absorbers necessary to shield the critical superconducting coils in the cold section and then to place *passive* absorbers in the straight section for the protection of highly irradiated warm magnets. Next, the heat deposition in the cold part was recomputed to account for the correction introduced by the presence of the passive absorbers of the straight section. This calculation contained the corrected description of the TCP, whose active jaws had been extended in the meantime from 20 to 60 cm. From the first calculations it was observed that the horizontal beam loss scenario was the most harmful for the cold magnets so in order to limit the CPU usage, it was the only case considered most of the time. This hypothesis, however, was validated at the end of the decision scheme by checking the doses of the final setup with the vertical and skew beam loss scenarios. Moreover, the irradiation for the injection is reported in Section 5.

Thus, the simulations are organized as follows:

1. Calculation of heat deposition in the cold section without protection, 20 cm TCP.
2. Optimization of active absorbers in the cold section, 20 cm TCP.
3. Optimization of passive absorbers in the straight section, 60 cm TCP.
4. Re-calculation of heat deposition in cold section with passive absorbers, 60 cm TCP.
5. Refinement of calculations (taking into account the halo impact in the active absorbers) and special cases (secondary collimators off).

Details of the simulation setup can be found in [4].

1.4 Normalization of the results

The energy density $\left[\frac{GeV}{cm^3\ p}\right]$ results obtained from FLUKA simulations were transformed into power densities $\left[\frac{W}{cm^3}\right]$ by the following factors $Fn\left[\frac{J\ p}{GeV\ s}\right]$:

Top energy, nominal conditions $Loss\ rate = 4.0 \cdot 10^{11}\ \left[\frac{p}{s}\right] \Rightarrow Fn = 64.0$

Injection, nominal conditions $Loss\ rate = 8.6 \cdot 10^{11}\ \left[\frac{p}{s}\right] \Rightarrow Fn = 137.6$

Where the loss rates are given assuming a 0.2 h and 0.1 h beam lifetime at nominal intensity for fully squeezed and injection optics, respectively [5][1].

For the commissioning scenario with TCS's open, a further factor of 0.15 has to be applied to account for the fact that the beam will carry (less than) 15% of the nominal intensity.

NOTE THAT ALL THE FOLLOWING RESULTS HAVE TO BE INTERPRETED QUALITATIVELY AND NEVER LITERALY SINCE, IN ADDITION TO LARGE STATISTICAL ERRORS, IMPORTANT SYSTEMATIC UNCERTAINTIES AFFECT THE CALCULATIONS. When simulating the cascade induced by 7 TeV beam protons lost in the collimator jaws, these are carried by i. loss assumptions, ii. grazing impacts (the jaw surface roughness is not taken into account), iii. FLUKA models and cross section extrapolation at 7 TeV, iv. geometry and material implementation and large distances between collimators and concerned magnets (implying a dramatic dependence on a tiny fraction of solid angle in the angular distribution of the reaction products), v. estimation of quench limits... For the sources of error ii-iv, factors of 2, 1.3 and 2, respectively, can be taken as a safe choice.

1.5 Candidate absorbers

Optimum solutions were sought among a set of configurations (see Table 3 and Fig. 1) that resulted from taking several variables into account:

Position of the TCLA's. Seven candidate positions negotiated with the beam integration group were allocated for the TCLA's; *A4* and *A6* between the interaction point IP7 and the first downstream dogleg bending magnet MBW.A6R7.B1, *B6* between the two downstream dogleg bending magnet pairs, *C6* and *F6* after the second downstream dogleg bending magnet pair but upstream of the MQT6 group, and *A7 or B7* between MQT6 and the DS.

Orientation of the absorbers. Two orientations are considered, *horizontal* and *vertical*.

Jaw Material. Both full copper and copper with a tungsten insertion (W) were suggested.

[1] These numbers may have been refined since the completion of our computations.

Absorber	$A4_{v/h}$	$\mathbf{A6}_v$	$\mathbf{B6}_h$	$\mathbf{C6}_v$	$\mathbf{F6}_h$	$\mathbf{A7}_h$	$B7_{v/h}$
Position abs.$[m]$	20022.5	20148.3	20179.3	20213.1	20216.1	20232.1	20243.9
Position-IP7 $[m]$	28.37	153.927	184.801	218.352	220.351	237.698	249.781
Orientation	V/H	V	H	V	H	H	V/H
Half gap $[\mu m]$	$10\,\sigma_{y/x}$	1585	2840	2787	1779	1788	$10\,\sigma_{y/x}$

Table 3: Summary of the properties of the **selected** and *discarded* absorbers.

Beam loss scenario. Three scenarios are considered: Mainly horizontal losses (H), vertical losses (V) or skew losses (S).

"Brute-force" examination would have required too much CPU so educated shortcuts were taken once the trends examined.

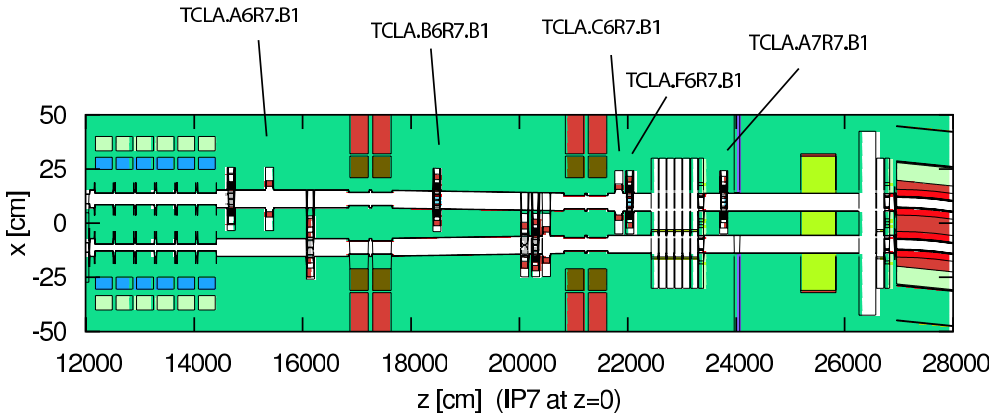

Figure 1: Schematic layout of the finally selected absorbers along IR7 beam1.

2 Protection of Q6

A preliminary set of simulations scanned through the efficiency of the first 5 TCLA positions in terms of the power density computed for the coils of the MQT6 group and, in particular, for the first component: MQTLH.A6R7.B1 (see appendix, A.3).

A4 was soon discarded (too far away), while *A6*, *B6* and *C6* were retained. Moreover, it was verified that an alternating angle scheme was best filtering the showers, so the starting configuration was frozen as $A6_vB6_hC6_v$[2]. Initially, when

[2](v) stands for vertical and (h) for horizontal orientation of the TCLA's.

TCS	TCP	TCLA	A4	A6	B6	C6	F6	MQT6
100	20	Cu						850
			h					∼850
			v					650
				h				550
				v				700
					h			170
					v			300
						h		700
						v		80
				v	h			5.5
					h	v		2.2
				v	h	v		1.7
					h	v	h	1.3
				v	h	v	h	0.77
		W		v	h	v	h	0.22
	60	W		v	h	v	h	0.85
0	60	W		v	h	v	h	*30*

Table 4: SCENARIO: horizontal losses at top energy and nominal conditions. Power density peaks [$\frac{mW}{cm^3}$] in the coils of MQTLH.A6R7.B1. Last line corresponds to a commissioning scenario where the TCS are retracted and, thus, the power density of 30 $\frac{mW}{cm^3}$ has to be weighted by the 0.15 factor, as indicated in 1.4. The two last lines include passive absorbers.

5 $\frac{mW}{cm^3}$ was taken as threshold, 3 TCLA's alone could comply with specifications (peak of $\sim$ 1.7 $\frac{mW}{cm^3}$), but after the establishment of the more stringent level of 1 $\frac{mW}{cm^3}$, it became clear that a fourth absorber ($F6_h$) would be needed to shield MQTLH.A6R7.B1 with some confidence. The resulting configuration ($A6_vB6_hC6_v$ $F6_h$) indeed reduced the peak density in MQT6 down to about 0.77 $\frac{mW}{cm^3}$, still allowing a relatively scarce margin for contingencies. Improvements were then tentatively looked for by rerunning simulations with W insertions in the Cu jaws. Results proved enormously encouraging, with peak power densities as small as 0.22 $\frac{mW}{cm^3}$.

However, that was not the end of the story. Two major changes took place shortly after: first, passive absorber blocks were introduced in the straight section [6] and, second, the active length of the jaws of the primary collimators was changed from 20 to 60 cm, which finally raised the dose in MQT6 by a factor of 4, up to 0.85 $\frac{mW}{cm^3}$. The results of the successive simulations can be followed in

Table 4.

† The W insertion in the Cu jaws reduces the peak heat deposition in MQT6 by almost a factor of 4.

† The dose in MQT6 with the 60 cm long TCP jaws is four times higher than that with the 20 cm long jaws.

3 Protection of the DS

The previous situation left one active absorber available at *A7* or *B7* to provide extra shielding for the MQ's and MB's of the DS. Simulations were carried out for each of the two positions with horizontal and vertical jaws and the goodness of each solution was judged through the total and peak doses in MQ7-MQ13 and MB.A8R7.B1-MB.C13R7.B1. The best solutions, equivalent within statistical fluctuations, were those containing $A7_h$ or $B7_h$, compared in Fig. 2.

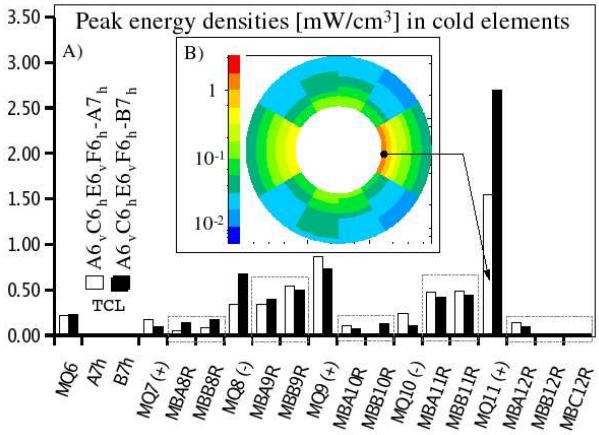

Figure 2: A.) Peak power density $[\frac{mW}{cm^3}]$ in MQ's and MB's for $A7_h$ (□) and for $B7_h$ (■). In the legend, old naming applies: TCL reads TCLA, $C6_h$ reads $B6_h$, and $E6_v$ reads $C6_v$. B.) Power density in MQ11.

The magnetic field was refined several times for an optimum tracking in the MB's, but the results remained stable in the range of small corrections, which affirmed the confidence in the calculations. Moreover, Fig. 2A seems coherent with the expected beam optics, with a broader horizontal beam (and thus higher doses) in the MB's that follow an h-defocusing quadrupole (-). It is remarked that not only the doses remain mainly under the quench limits, with the exception of MQ11, but

also the z-derivatives show that the beam delivered beyond IR7 should not be destructive[3]. For MQ11 (see Fig. 2A and B), however, special actions may have to be taken in the future.

Table 5 summarizes the study on peak power densities ($[\frac{mW}{cm^3}]$) in the MB's and MQ's. Column 2 deals with integrally copper TCLA jaws, while the other columns display the result for the W insertion case. From column 4 onwards simulations were performed with the 60 cm active length TCP's. Column 6 describes the accident case when the TCS are retracted, and column 5 shows the contribution of the direct impacts in the TCLA's, highlighted also in Fig.3.

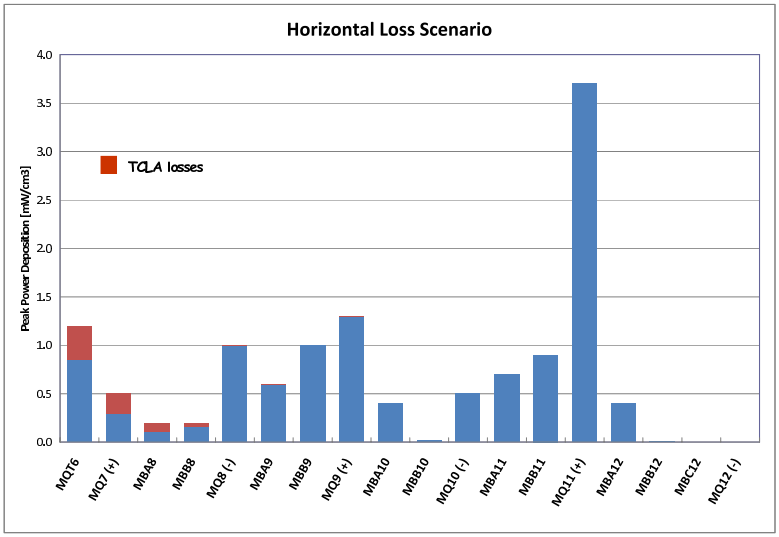

Figure 3: Peak power densities $[\frac{mW}{cm^3}]$ in MQ's and MB's for the adopted TCLA configuration ($A6_vB6_hC6_vF6_hA7_h$). The contribution of losses in the active absorbers is indicated in red.

† In the horizontal loss scenario, higher peak power densities are found for objects immediately downstream a h-defocusing MQ.

† For MQ's the peak power densities are around the expected quench limit, substantially exceeded in the case of MQ11, which is the most affected magnet.

[3]Detailed scoring of particles originated from non-elastic collisions of the beam halo in the collimators and predicted to leave MBC13 inside the beam 1 vacuum chamber, has been performed to allow their further tracking by optics colleagues.

1	2	3	4	5	6	
TCP jaws	20 cm	20 cm	60 cm	60 cm	60 cm	1
TCLA jaws	Cu	Cu+W	Cu+W	Cu+W	Cu+W	2
TCS	ON	ON	ON	ON	OFF	3
5^{th} TCLA	$B7_v$	$A7_h$	$A7_h$	$A7_h$	$A7_h$	4
PA	OFF	OFF	ON	ON	ON	5
losses in TC...	P+S	P+S	P+S+LA	LA	P+LA	6
MQT6	0.77	0.22	1.2	0.35	29.9	7
MQ7	0.46	0.18	0.5	0.21	2.4	8
MBA8	0.10	0.05	0.2	0.09	1.7	9
MBB8	0.32	0.09	0.2	0.04	0.5	10
MQ8	0.88	0.35	1.0	5E-3	0.4	11
MBA9	0.60	0.35	0.60	3E-3	0.8	12
MBB9	0.54	0.55	1.0	1E-3	1.0	13
MQ9	0.35	0.88	1.3	2E-3	2.4	14
MBA10	0.08	0.12	0.4	$\sim$0	0.3	15
MBB10	4E-3	0.02	$\sim$0.02	$\sim$0	0.1	16
MQ10	0.16	0.24	0.5	$\sim$0	0.3	17
MBA11	0.37	0.48	0.7	1E-3	1.3	18
MBB11	0.38	0.49	0.9	1E-3	1.5	19
MQ11	2.56	1.55	3.7	$\sim$0	3.7	20
MBA12	0.10	0.14	$\sim$0.4	$\sim$0	0.2	21
MBB12	1E-3	0.01	$\sim$5E-3	$\sim$0	$\sim$0	22
MBC12	-	$\sim$0	$\sim$0	$\sim$0	$\sim$0	23
MQ12	0	0	0	0	$\sim$0	24

Table 5: Peak power densities $[\frac{mW}{cm^3}]$ in the DS for the horizontal beam loss scenario at 7 TeV (**lwb**). Five *active* absorbers (**TCLA**) are on, $A6_vB6_hC6_vF6_h$ (chosen in Sec. 2) + 5^{th} absorber (row 4), and sometimes (row 5) also the *passive* absorbers (**PA**). As for the loss source (row 6), simulations were first computed for losses originated in the TCP's and TCS's only. Then the contributions from the TCLA's were included. Column 6 represents the commissioning case where the TCS's are off (a reduction factor of 0.15 needs then to be applied to account for the reduced intensity during commissioning).

4 Hadronic shower generated in the active absorbers

As discussed in the previous sections, some of the active absorbers have been placed in front of the first superconducting magnets in order to shield them from the hadronic shower generated upstream in the tunnel. The half-gap of the jaws is at 10 σ_r with respect to the beam profile; this value is relatively high compared to the one of the primary (6 σ_r) and secondary (7 σ_r) collimators. Such a large aperture guarantees a fairly low, though non-zero number of primary proton-TCLA collisions. In fact, the showers originated upon the rare beam halo interception events in the TCLA jaws, could have significant impact in the superconducting objects close-by. In order to evaluate this additional risk of magnet quenching, the study could be divided into two steps: estimating the peak energy deposition in the magnets per primary proton lost in the active absorbers and scaling by the TCLA loss rate.

4.1 First order calculations

Dedicated FLUKA simulations were run with a source of particles uniformly distributed over the inner (exposed to the beam) thin layer of the absorber jaws. It was found that if the beam losses in the absorber correspond to 0.1% of the total losses in the collimators, then the peak density raised in the superconducting coils would be around 1 $\frac{mW}{cm^3}$, which is comparable to the contribution from the collimator losses.

4.2 Refined calculations

Only after having frozen the positions of the five active absorbers, the beam tracking codes could be rerun to obtain the new proton interactions. The new file essentially is comparable to the old one, with the exception of a few interaction events in the newly introduced active absorbers[4].

From the fresh interaction file a new source file that included all interactions (in collimators and absorbers) could be generated and the doses could be recomputed as in the previous sections. However, since the fraction of interactions in the absorbers is very little and the statistical fluctuation of the results rather big, it would be quite difficult to tell what is the contribution of the showers coming from interactions in the absorbers to the total peaks in the cold arc. Thus, a set of simulations was launched with a source file filtered exclusively in the active absorbers,

[4]Indeed, for multi-turn computations a particle intercepted in the TCLA's will follow a different path through the "old" elements, so the effect is not exclusively seen in the TCLA's but also, though moderately, in the other objects.

and the results were accordingly weighted (to the likeliness of such collisions).

The number of interactions in the TCLA's for the given input (horizontal losses at top energy) was 845 out of 1242331 interactions everywhere. The contribution of the showers induced by the proton impacts in the active absorbers, scaled by $\frac{845}{1242331} = 6.8 \cdot 10^{-4}$, appears in the 5^{th} column of Table 5 and is shown in Figure 3 as a part of peak power densities eventually expected (4^{th} column of Table 5). The increase of dose is compatible, though less important, than the one predicted in the first order calculation where the number of impacts in the TCLA's was tentatively taken as 0.1% while beam tracking calculations cast 0.07 $\%$.

5 Other potentially harmful beam loss scenarios

The first calculations determined that the horizontal loss scenario was the worst in terms of peak dose in the cold section. However, a few variables changed from the initial calculations, and others were not even considered. For example, the active length of the primary collimators was extended from 20 to 60 cm, passive absorbers were inserted, and the halo impact in the active absorbers was included in the beam interaction files. These changes justify to check the final power deposition also in the vertical beam loss scenario. Other scenarios that are surveyed are those that occur during injection and the commissioning mode where the TCS's are retracted. Results are summarized in Table 6.

5.1 Vertical and skew beam loss scenarios at top energy

Table 7 serves to compare the peak power densities in MQT6 and DS magnets at low beta (beam energy of 7 TeV) for horizontal, vertical and skew beam loss scenarios at nominal intensity.

Except for the hottest object, MQ11, which registers similar values for the horizontal and vertical cases, the horizontal loss scenario seems the most hazardous one, as anticipated in the early calculations.

5.2 Commissioning case at top energy

This section reviews the case where the secondary collimators are open. Thus the active absorbers are left to capture the secondary and tertiary halo. From COLLTRACK [7] calculations, both for the horizontal and vertical loss scenarios at low beta in this mode, the number of interactions in the active absorbers can rise by up to 5 orders of magnitude with respect to those in nominal operation. Among the active absorbers the biggest source of shower is TCLA.B6.

1	2	3	4	5	6	7	8	9	
E [GeV]	7000	7000	7000	7000	7000	450	450	450	1
TCS	ON	ON	OFF	ON	OFF	ON	OFF	OFF	2
TCLA	OFF	ON	ON	ON	ON	ON	ON	ON	3
Losses	Hori	Hori	Hori	Vert	Vert	Hori	Hori	Vert	4
MQT6	350	1.2	29.9	0.25	39.3	∼0.2	5.5	12.5	5
MQ7	39	0.5	2.4	0.1	2.6	∼0.02	0.7	<0.9	6
MBA8	11	0.2	1.7	0.3	2.6	∼0.09	0.1	<0.05	7
MBB8	13	0.2	0.5	0.03	∼1	∼0.02	<0.11	∼0.05	8
MQ8	5	1.0	0.4	0.20	∼5	∼0.07	∼0.10	∼0.07	9
MBA9	2	0.60	0.8	0.22	1.5	∼0.02	∼0.03	∼0.03	10
MBB9	1.3	1.0	1.0	0.27	1.5	∼0.02	∼0.07	∼0.10	11
MQ9	1.0	1.3	2.4	0.29	1.7	∼0.01	∼0.03	<0.03	12
MBA10	0.24	0.4	0.3	0.06	∼0.5	<0.02	<0.05	<0.07	13
MBB10	0.01	∼0.02	0.1	0.12	∼0.02	∼2E-3	<0.05	<0.07	14
MQ10	0.55	0.5	0.3	1E-3	∼0.5	∼0.02	∼0.07	<0.07	15
MBA11	1.8	0.7	1.3	0.39	1.8	∼0.01	∼0.05	∼0	16
MBB11	1.7	0.9	1.5	0.25	2	∼0.01	∼0.05	∼0	17
MQ11	6.6	3.7	3.7	3.6	∼7	∼0.05	∼0.07	∼0	18
MBA12	0.19	∼0.4	0.2	0.14	0.7	∼2E-3	∼0	∼0	19
MBB12	∼1E-3	∼5E-3	∼0	∼0.02	∼1E-3	∼0	∼0	∼0	20
MBC12	0	∼0	∼0	∼5E-3	∼0	∼0	∼0	∼0	21

Table 6: Peak power densities $[\frac{mW}{cm^3}]$ in the DS for injection and top energy (*row 1*), with horizontal or vertical beam losses (*row 4*). Five *active* absorbers (**TCLA**), $A6_vB6_hC6_vF6_hA7_h$ (chosen in Secs.2 and 3) are on or off (*row 3*) and *passive* absorbers (**PA**, see [6]) are included. *Row 2* distinguishes the commissioning mode where the TCS's are retracted (OFF) for which a further 0.15 factor has to be applied to account for reduced intensity.

1	2	3	4
Losses	**hori**	**vert**	**skew**
MQT6	1.2	0.25	0.20
MQ7	0.5	0.1	0.1
MBA8	0.2	0.3	0.05
MBB8	0.2	0.03	$\sim$0
MQ8	1.0	0.20	0.03
MBA9	0.60	0.22	0.23
MBB9	1.0	0.27	0.36
MQ9	1.3	0.29	0.59
MBA10	0.4	0.06	0.05
MBB10	$\sim$0.02	0.12	0.01
MQ10	0.5	1E-3	$\sim$0
MBA11	0.7	0.39	0.23
MBB11	0.9	0.25	0.30
MQ11	3.7	3.6	1.1

Table 7: Peak power densities $[\frac{mW}{cm^3}]$ in the DS at top energy and nominal conditions for three beam loss scenarios: **hori**zontal, **vert**ical and **skew**.

In nominal operation, where the active absorbers count no more than 1 ‰ of the total interactions, their showers lead to peak power densities in MQ6 and MQ7 equal to 30-40 % of the peaks predicted including TCP and TCS losses[5]. Thus, this mode could be expected to quench the magnets. However, a specification for the commissioning scenario is that the loss rate stays below 15 % of the nominal one (see Sec. 1.4 on page 5).

Simulations for the horizontal/vertical loss scenarios cast the results listed in columns 4/6 of Table 6.

5.3 Losses at injection (450 GeV)

At injection the beam spot is broader and the loss rates are higher. The collimators and absorbers are adapted to the beam actual σ_r at each location. The densities of power deposited in the cold section for horizontal losses at injection with all protection devices, i.e. collimators, on (nominal conditions), are well below those registered at top energy (compare columns 7 and 3 in Table 6).

Results for TCS retracted can be found in the two rightmost columns of Table 6.

[5] As shown in Figure 3.

6 Conclusions

6.1 Power deposition in MQT6

The results of the studies of peak power deposition in MQT6 (see Sec. 2) are collected in Table 4.

† The W insertion in the Cu jaws reduces the peak deposition in the MQT6 group by almost a factor of 4.

† The dose in MQT6 with the 60 cm long TCP jaws is four times higher than that with the 20 cm long jaws.

6.2 Power deposition in the Dispersion Suppressor

The results of the studies of peak power deposition in MQ7-MQ12 (see Sec. 3) are collected in Tables 5-7.

The contribution of the beam halo impact in the active absorbers is significant (30-45 %) for the peak power densities of MQT6, MQ7 and MBA8, then it damps immediately.

6.3 Other scenarios

Looking at Table 6, we can conclude what follows:

† The peak power densities at controlled injection (TCS's and TCLA's on, *column 7*) are expected to not compromise the superconduction in the magnets.

† The mode in which the secondary collimators (TCS) are retracted (*columns 4, 6, 8* and *9*) would produce a quench in MQT6 at top energy (peak power deposition p_{7TeV} of 30-40 $\frac{mW}{cm^3}$) and most likely also at injection ($p_{450GeV} \simeq 6-13\ \frac{mW}{cm^3}$) for nominal intensity, but not for commissioning conditions (<15 % of nominal intensity). The first three magnets (MQT6, MQ7, MBA8) absorb most of the additional radiation so that the effect damps quickly and the rest of the DS turns out to be unaffected.

† The failure mode in which the jaws of the active absorbers (TCLA) are retracted (*column 2*) would be quite severe, the peak power density in MQT6 reaching 350 $\frac{mW}{cm^3}$.

† At top energy and normal operation, the horizontal beam loss scenario is more harmful than the vertical and skew ones. The most irradiated object in

all cases is MQ11, with almost identical expectations for the horizontal and vertical loss patterns (3.7 and 3.6 $\frac{mW}{cm^3}$, respectively).

A Scoring and post-processing technicalities

A.1 Scoring in the MQ's

The USRBIN output stored in the unit 28 gives a radial-azimuthal-longitudinal scoring (with 10 radial, 12 angular and 31 longitudinal divisions) of the energy deposited in MQ7R-MQ13R coils (7 separate binnings).

```
***** MQ.7R7.B1
** 7. Beam 1, coil C5B1COIL
USRBIN          11.     ENERGY      -28.0        6.        0.      155.MQ7R
USRBIN        2.80        9.7       -155.       10.       12.       31.&
**
***** MQ.8R7.B1
** 7. Beam 1, coil C5B1COIL
USRBIN          11.     ENERGY      -28.0        6.        0.      155.MQ8R
USRBIN        2.80        9.7       -155.       10.       12.       31.&
...
```

A.2 Scoring in the MB's

The USRBIN output stored in the unit 32 gives a radial-azimuthal-longitudinal scoring (with 10 radial and 9 angular divisions and z-divisions every $\sim$9 cm) of the energy deposited in the coils of MBA8R, MBB8R; MBA9R, MBB9R; MBA10R, MBB10R; MBA11R, MBB11R; MBA12R, MBB12R, MBC12R; MBA13R, MBB13R, MBC13R[6]. The magnets have a bend, which in the FLUKA geometry has been implemented by chopping the MB's in *four* cylinders. *Three* USRBIN binnings have been set for each magnet, one for the first quarter, another for the medium half and the last for the last quarter of the magnet. In total there are $3 \cdot 14 = 42$ binnings inside the USRBIN unit 32. The axes of the cylindrical meshes do not match exactly the cylinder axes, as illustrated in Fig. 4[7].

```
****  MB.A8R7.B1
* 1. Beam 1, section a
USRBIN          11.     ENERGY      -32.0       6.00        0.     -357.MBA8R
USRBIN         2.5       10.04       -715.       10.        9.       40.&
* 1. Beam 1, section b and c
USRBIN          11.     ENERGY      -32.0       6.00        0.      357.MBA8R
USRBIN         2.5       10.40       -357.       10.        9.       80.&
* 1. Beam 1, section  d
```

[6]Note that MB12 and MB13 are triplets.

[7]Note that both for the MQ's and the MB's the scoring is done in a cylindrical collar around the pipe which includes not only the coils but also other objects. This is a conservative simplification.

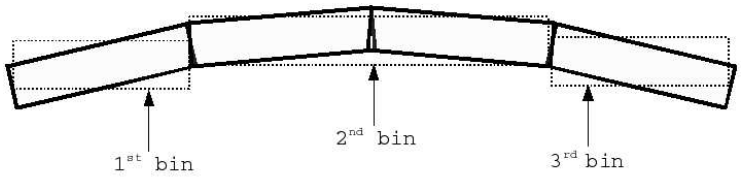

Figure 4: Sketch of the MB FLUKA implementation in 4 cylinders and of the corresponding scoring meshes, 1 and 3 for the extremes and 2 for the central part.

```
USRBIN          11.     ENERGY      -32.0       6.00        0.       715.MBA8R
USRBIN         2.5       10.04       357.        10.        9.        40.&
*
****  MB.B8R7.B1
* 1. Beam 1, section a
USRBIN          11.     ENERGY      -32.0       6.00        0.      -357.MBB8R
USRBIN         2.5       10.04       -715.       10.        9.        40.&
* 1. Beam 1, section b and c
USRBIN          11.     ENERGY      -32.0       6.00        0.       357.MBB8R
USRBIN         2.5       10.40       -357.       10.        9.        80.&
* 1. Beam 1, section  d
USRBIN          11.     ENERGY      -32.0       6.00        0.       715.MBB8R
USRBIN         2.5       10.04       357.        10.        9.        40.&
...
```

A.3 Scoring in MQT6 and MCBC

The USRBIN output stored in the unit 33 gives a radial-azimuthal-longitudinal scoring (with 1 radial and 20 angular divisions and z-divisions every 10 cm) of the energy deposited in the coils of MQTLH.A6R7.B1, MQTLH.B6R7.B1 and MQTLH.C6R7.B1 (some other binnings exist but are usually inactive), and also of MCBCV.6R7.B1.

```
* 1. Beam 1, coil C1B1COIL
USRBIN          11.     ENERGY      -33.0       3.57        0.        65.MQTLHA6R
USRBIN        2.32        9.7        -65.          1.       20.        13.&
...
*** MCBCV.6R7.B1
* 13. Beam 1, coil C2B1COIL
USRBIN          11.     ENERGY      -33.0       3.85        0.        45.MCBCV6R
USRBIN        2.82        9.7        -45.          1.       20.         9.&
...
```

A.4 Re-binning of the results

The energy deposition events in the DS are so rare that collecting statistics in a fine mesh results into a blurry/spiky image. In order to stabilize the results, these

were re-binned into bigger portions of volume. The re-binning factors were chosen as a compromise between acceptable statistics and peak resolution, and were the following ones (n stands for new binning and o for old binning):

- For USRBIN 28 (MQ's) $(\Delta r)_n/(\Delta r)_o = 2$ and $(\Delta\phi)_n/(\Delta\phi)_o = 3$
- For USRBIN 32 (MB's) $(\Delta r)_n/(\Delta r)_o = 2$, $(\Delta\phi)_n/(\Delta\phi)_o = 3$ and $(\Delta z)_n/(\Delta z)_o = 2$
- For USRBIN 33 (only MQTLH6) $(\Delta\phi)_n/(\Delta\phi)_o = 5$

The script *rebin.sh* produces a list with all the results in the given directory and runs the program *ubredu_stat* with the re-binning factors specified above. The ".rb" suffix is appended to the name of the re-binned output files.

A.5 Peak detection and parsing scripts

The script *anMBMQ.sh* produces the table *LatticeWatt*, listing total power deposition for each geometry region, and the table *results*, giving peak power deposition in the superconducting coils. The second table is gotten by averaging the different results, re-binned or original, and thereafter parsing values from the summary files (such as *usrbin_28*), whereas the first implies that the *EnLattice.pl* code is internally called.

A typical *results* table is shown below (note that the units for all numbers quoted as "max" are mW/cm^3).

```
/home/LHC/IR7/TCP60new/hori/NoTCL/COLD_SECTION
Number of simulations: 25
******* Straight Section *************
**    * MQTLHA6R ********************
      * max heat in coil:........   350.580 mW (+-     7.90 %)
      * Total heat in the coil:..   130.40  W  (+-     5.00 %)
      * heat in MQ:..............   331.22  W  (+-     4.20 %)
**    * MQ6 group ******************
   MQTLHA6R    331.22 (+-     4.20 %) W
   MQTLHB6R     32.00 (+-     4.36 %) W
   MQTLHC6R     15.00 (+-     5.35 %) W
   MQTLHD6R     12.19 (+-     6.39 %) W
   MQTLHE6R     12.06 (+-     7.62 %) W
   MQTLHF6R     12.00 (+-     8.29 %) W
  -------------------------------------
      TOTAL      390.41 (+-     3.59 %) W
******* Curved Section *************
Total energy in coils and magnets of MQ[7-11]R.
   MQ7   | max: 39.433 (+-17.5%) |  7.075e+01  +- 11% |  Total: 117.5  W   +- 7.27 %
   MQ8   | max: 4.626 (+-63.3%)  |  1.590e+01  +- 22% |  Total: 27.89  W   +- 13.7 %
   MQ9   | max: 0.974 (+-57.3%)  |  2.338e+00  +- 46% |  Total: 4.004  W   +- 28.4 %
   MQ10   | max: 0.541 (+-89.5%) |  3.154e-01  +- 73% |  Total: 0.5320 W   +- 46.1 %
   MQ11   | max: 6.582 (+-55.2%) |  7.697e+00  +- 46% |  Total: 11.95  W   +- 31.3 %
```

```
   MQ12   | max: 0.000 (+-0.0%) |  |  Total: 0 W   +- 0 %
   MQ13   | max: 0.000 (+-0.0%) |  |  Total: 0 W   +- 0 %
Total energy in coils and magnets of MB[A-B][8-11]R.
   MBA8R   | max: 3.177 (+-22.4%) 11.102 (+-14.8%) 9.491 (+-16.4%) | 1:MB_CO1C2: ...
   MBB8R   | max: 13.201 (+-15.0%) 2.570 (+-32.9%) 1.666 (+-59.0%) | 2:MB_CO1C2: ...
   MBA9R   | max: 2.025 (+-38.4%) 1.895 (+-48.8%) 0.605 (+-41.5%)  | 3:MB_CO1C2: ...
   MBB9R   | max: 1.223 (+-47.3%) 1.336 (+-62.2%) 0.964 (+-43.5%)  | 4:MB_CO1C2: ...
   MBA10R  | max: 0.235 (+-70.4%) 0.086 (+-99.3%) 0.124 (+-99.9%)  | 5:MB_CO1C2: ...
   MBB10R  | max: 0.009 (+-69.8%) 0.001100.0 (+-%) 0.000 (+-0.0%)  | 6:MB_CO1C2: ...
   MBA11R  | max: 1.822 (+-67.0%) 1.002 (+-93.9%) 0.762 (+-74.6%)  | 7:MB_CO1C2: ...
   MBB11R  | max: 1.208 (+-78.0%) 1.663 (+-83.9%) 0.444 (+-82.0%)  | 8:MB_CO1C2: ...
   MBA12R  | max: 0.190 (+-70.3%) 0.060 (+-99.7%) 0.000100.0 (+-%) | 9:MB_CO1C2: ...
   MBB12R  | max: 0.001100.0 (+-%) 0.000 (+-0.0%) 0.000 (+-0.0%)   |10:MB_CO1C2: ...
   MBC12R  | max: 0.000 (+-0.0%) 0.000 (+-0.0%) 0.000 (+-0.0%) |  |
   MBA13R  | max: 0.000 (+-0.0%) 0.000 (+-0.0%) 0.000 (+-0.0%) |  |
   MBB13R  | max: 0.000 (+-0.0%) 0.000 (+-0.0%) 0.000 (+-0.0%) |  |
   MBC13R  | max: 0.000 (+-0.0%) 0.000 (+-0.0%) 0.000 (+-0.0%) |  |
```

The *results* table indeed displays also the total power in the coils of MQTLH.A6R7.B1, as well as that in each full element of the MQT6 group, with the sum (and the corresponding statistical errors in %).

As for MQ7-MQ13, the first column shows the peak power density, and the last two columns display the total power in the coils and in the full magnet. For each MB magnet, three peaks of power density are printed, corresponding to the three applied binnings (see Sec. A.2).

References

[1] A. Fassò, A. Ferrari, S. Roesler, P.R. Sala, G. Battistoni, F. Cerutti, E. Gadioli, M.V. Garzelli, F. Ballarini, A. Ottolenghi, A. Empl, and J. Ranft. The physics models of FLUKA: status and recent developments. In *Computing in High Energy and Nuclear Physics 2003 Conference (CHEP2003), La Jolla, CA, USA, March 24-28, 2003, (paper MOMT005), eConf C0303241 (2003), arXiv:hep-ph/0306267*, 2003.

[2] A. Fassò, A. Ferrari, J. Ranft, and P.R. Sala. *FLUKA: a multi-particle transport code*. CERN-2005-10, INFN/TC_05/11, SLAC-R-773, 2005.

[3] LHC Collimation Working Group. http://lhc-collimation.web.cern.ch/lhc-collimation.

[4] M. Magistris, M. Santana-Leitner, M. Brugger, F. Cerutti, A. Ferrari, and V. Vlachoudis. Technical description of the implementation of the IR7 section at LHC with the FLUKA transport code. Technical report, CERN-AB-ATB, 2008.

[5] M. Lamont. Estimates of annual proton doses in the LHC. LHC project note 375, CERN AB/OP, October 2005.

[6] R. Assmann and A. Ferrari. Addition of absorbers to IR7 and IR3. Engineering Change Order - Class I 692481, CERN, February 2006.

[7] G. Robert-Demolaize, R. Assmann, S. Redaelli, and F. Schmidt. A New Version of SixTrack with Collimation and Aperture Interface. In *PAC05 proceedings*. CERN, 2005.